Electronic Supplementary Material (ESI) for Dalton Transactions.

Supporting Information

Homoleptic Trimethylsilylchalcogenolato Zincates $[Zn(ESiMe_3)_3]^-$ and Stannanides $[Sn(ESiMe_3)_3]^-$ (E = S, Se): Precursors in Solution-Based Low-Temperature Binary Metal Chalcogenide and Cu_2ZnSnS_4 (CZTS) Synthesis

Jannick Guschlbauer, Tobias Vollgraff, Jörg Sundermeyer*

Fachbereich Chemie and Materials Science Center, Philipps-Universität, Hans-Meerwein-Str. 4, 35032 Marburg, Germany. *E-mail:JSU@staff.uni-marburg.de.

Content

1. Decomposition of [Sn(ESiMe$_3$)$_4$] (E = S (3), Se (4))

The TGA of [Sn(SSiMe$_3$)$_4$] (**3**) shows, that the investigated compound is not stable at ambient temperature, as a mass loss can be observed directly at the beginning of the measurement (**Figure S1**). When the first thermal process is finished at ca. 120 °C a plateau indicates a stable decomposition product that decomposes at ca. 550 °C, and a further decomposition at ca. 740 °C. It is assumed that a two-step elimination of two eq. of S(SiMe$_3$)$_2$ leads to SnS$_2$ (eq. S**1**). The TGA pattern above 550°C resembles that of the TGA of a SnS$_2$ reference reported in literature (eq. S**2**).[1] The decomposition from 740 °C on can be assigned to the thermolysis of SnS to the elements Sn and S (eq. S**3**).

$$\mathrm{Sn(SSiMe_3)_4} \rightarrow \mathrm{SnS_2} + 2\ \mathrm{S(SiMe_3)_2} \qquad \text{(S1)}$$

$$\mathrm{SnS_2} \rightarrow \mathrm{SnS} + \mathrm{S} \qquad \text{(S2)}$$

$$\mathrm{SnS} \rightarrow \mathrm{Sn} + \mathrm{S} \qquad \text{(S3)}$$

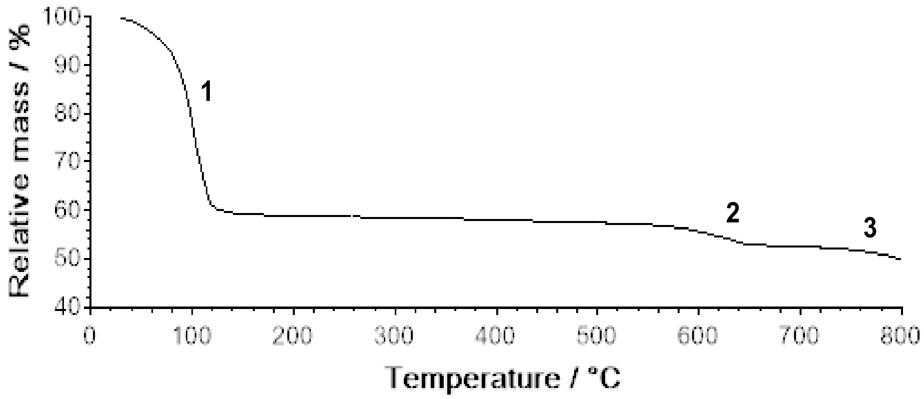

Figure S1: TGA of the assumed Sn(SSiMe$_3$)$_4$ (**3**) (heating rate of 10 K min^{-1}). The first decomposition (**1**) takes place at ambient temperature before the measurement starts. The second (**2**) and third (**3**) decomposition step is identical with the one, reported for SnS$_2$.[1]

Under different thermolysis conditions, decomposing [Sn(SSiMe$_3$)$_4$] (**3**) at 180°C and annealing the beige solid formed for 3 days, a black residue was formed identified as SnS in the Herzenbergite structure with minor impurities of SnS$_2$ in the berndtite structure via PXRD.

One possible explanation is the reductive elimination of the disulphide Me$_3$SiS-SSiMe$_3$ and subsequent elimination of S(SiMe$_3$)$_2$ to yield SnS. Obviously, there are two thermal pathways of decay possible depending on the heating rate: fast and constant heating leads to elimination of $S(SiMe_3)_2$ while isothermal decomposition at 180°C leads predominantly to $S_2(SiMe_3)_2$ and Sn(II). In any case, the TGA measurement of $Sn(SSiMe_3)_4$ does not indicate any direct (one step) transformation to SnS but rather SnS_2.

To investigate the first decomposition product a defined decomposition of the assumed $[Sn(SSiMe_3)_4]$ (**3**) was conducted by heating 100 mg of this compound at 180 °C under reduced pressure for approximately five minutes until no more volatiles are produced. The beige residue was annealed at 180 °C for 3 days and subsequently investigated via PXRD (**Figure S2**). The prepared material was identified as SnS in the Herzenbergite structure (JCPDS: 39-0354) with minor impurities of SnS_2 in the Berndtite structure (JCPDS: 21-1231).

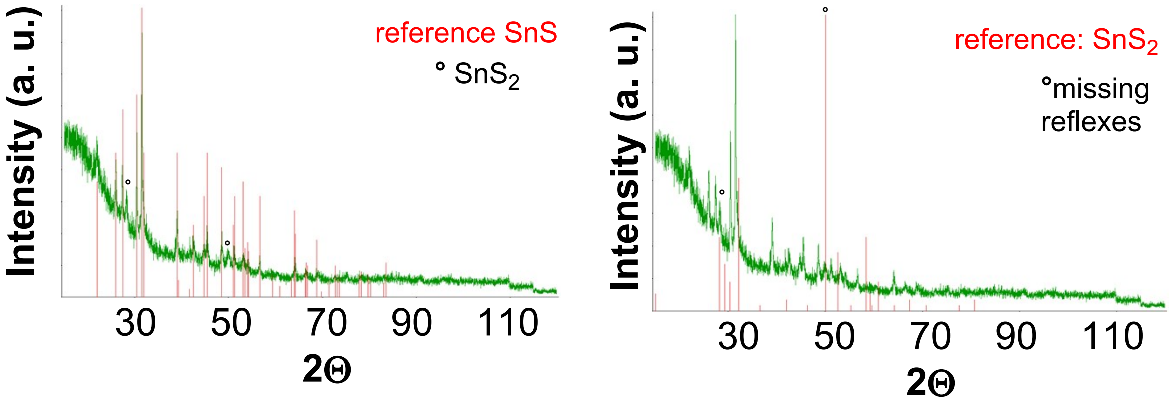

Figure S2: PXRD of the thermolysis product of the assumed $Sn(SSiMe_3)_4$. Top: the most reflexes are attributed to SnS in the herzenbergite structure (JCPDS: 39-0354). Bottom: reflexess that do not fit to the herzenbergite structure can be attributed to minor impurities of SnS_2 in the berndtite structure (JCPDS: 21-1231).

A possible explanation of the reduction of the tin centre is the reductive elimination of the silylated disulfide compound $Me_3SiS\text{-}SSiMe_3$.

To investigate the thermal decomposition product of the assumed selenium homologue $[Sn(SeSiMe_3)_4]$ (**4**) a defined thermolysis was conducted by heating a sample of 100 mg at 180 °C under reduced pressure for approximately five minutes until no more volatiles are produced. The black residue was annealed at 200 °C for 2 days and subsequently investigated via PXRD (**Figure S3**). The prepared material was identified as $SnSe_2$ (JCPDS: 89-3197) without any crystallographically active phase impurities. Compared to the decomposition of

$Sn(SSiMe_3)_4$, another decomposition mechanism without subsequent reduction has to take place obviously.

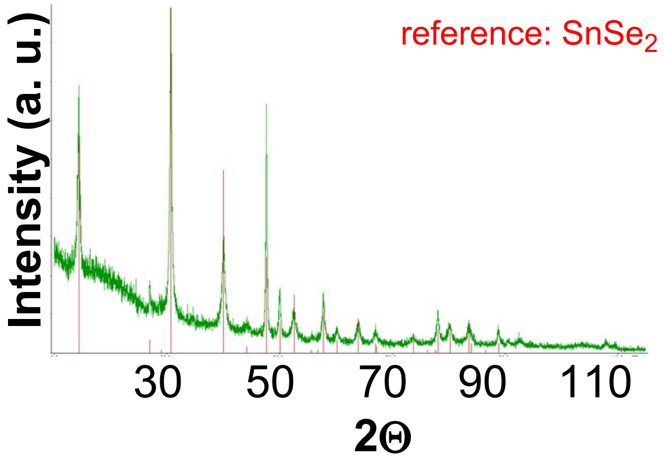

Figure S3: PXRD of the thermolysis product of the assumed $Sn(SeSiMe_3)_4$. After annealing at 200 °C for 2 days. The residue is identified as $SnSe_2$ (JCPDS: 89-3197).

2. NMR Spectra

2.1 NMR Spectra of $Ph_4P[Zn(SSiMe_3)_3]$ (1a)

Due to the poor solubility of 1a in THF the silicon grease contamination seems to be more severe than it is as proven by elemental analysis (attributed signals: δ_H = 0.11 ppm, δ_C = 1.1 ppm, δ_{Si} = –22 ppm).

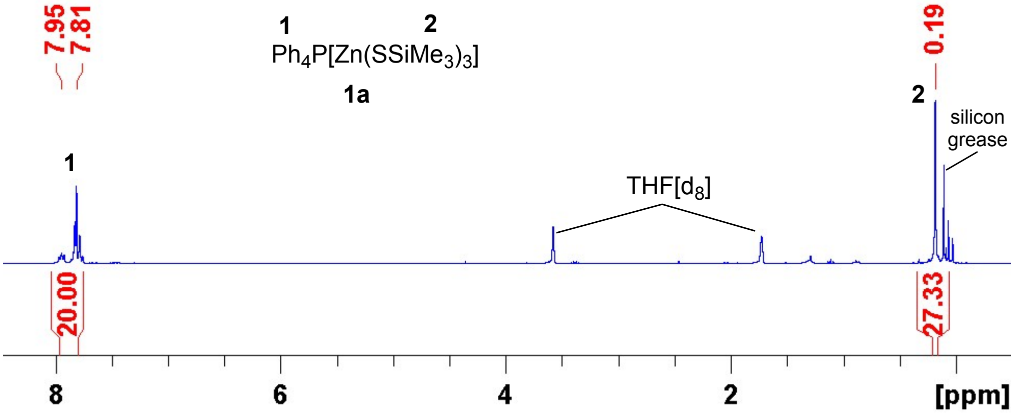

^{1}**H-NMR** (300.3 MHz, THF[d_8]) of **1a**. Note that the solubility of **1a** is very poor in thf.

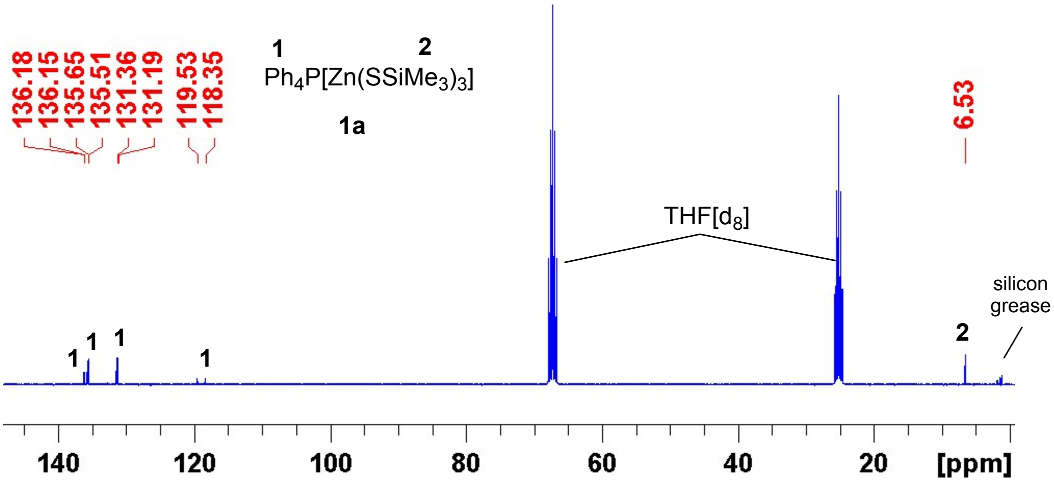

^{13}**C{^{1}H} NMR** (75.5 MHz, THF[d_8]) of **1a**. Note that the solubility of **1a** is very poor in thf.

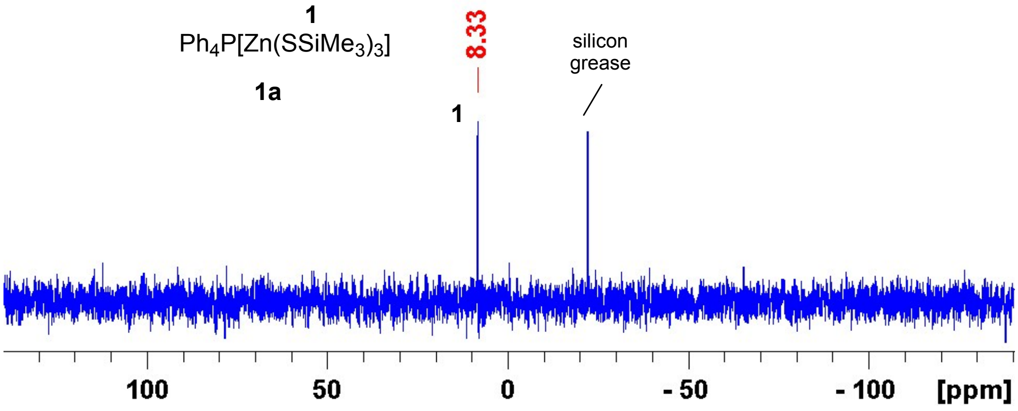

^{29}**Si-NMR** (59.7 MHz, THF[d$_8$]) of **1a**. Note that the solubility of **1a** is very poor in thf.

2.2 NMR Spectra of $Ph_4P[Zn(SeSiMe_3)_3] \cdot 0.5\ Et_2O$ (1b · 0.5 Et_2O)

Due to the poor solubility of 1b · 0.5 Et_2O in THF the silicon grease contamination seems to be more severe than it is as proven by elemental analysis (attributed singals: $\delta_H = 0.11$ ppm, $\delta_C = 1.1$ ppm, $\delta_{Si} = -22$ ppm).

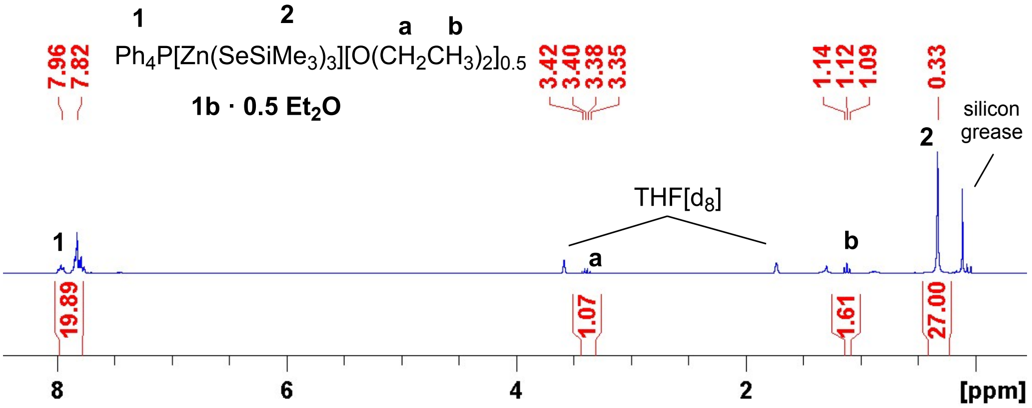

^{1}**H-NMR** (300.3 MHz, THF[d$_8$]) of **1b**. The solubility of **1b · 0.5 Et$_2$O** is very poor in thf.

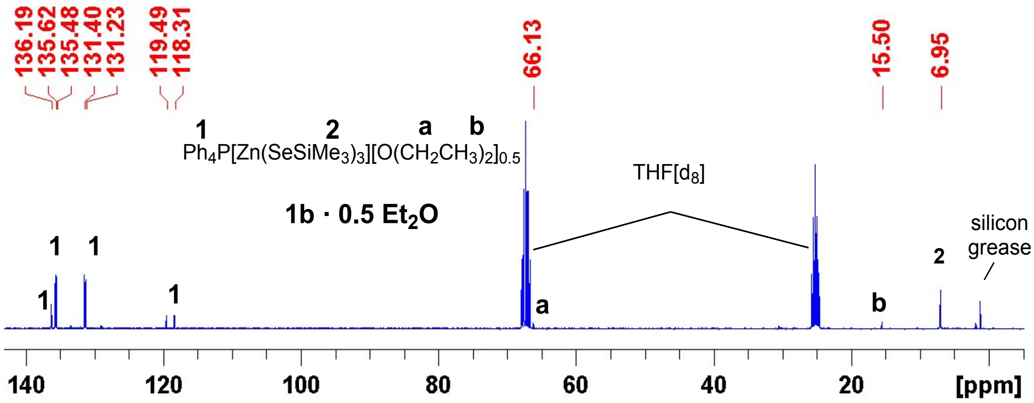

^{13}**C{^{1}H} NMR** (75.5 MHz, THF[d$_8$]) of **1b**. The solubility of **1b · 0.5 Et$_2$O** is very poor in thf.

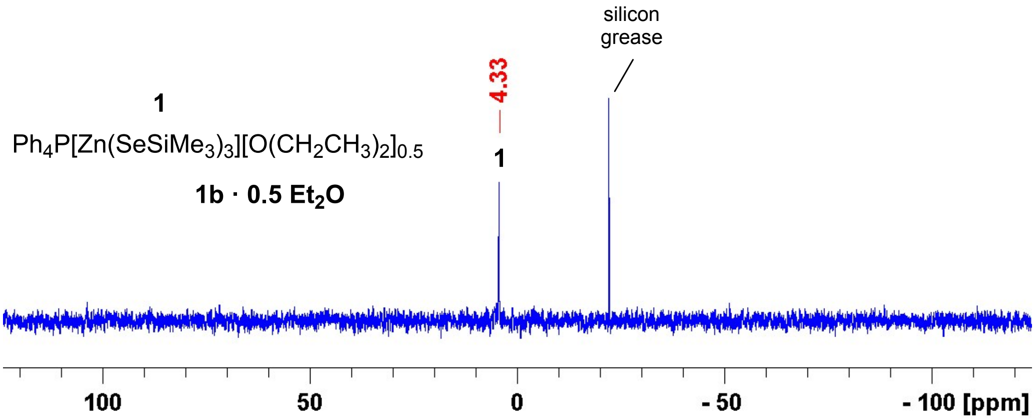

^{29}Si-NMR (59.7 MHz, THF[d_8]) of **1b**. The solubility of **1b · 0.5 Et_2O** is very poor in thf.

Several attempts to get a ^{77}Se-NMR spectrum of **1b** failed. We assume that the symmetrically coordinated zinc center causes problems. This is a commonly observed phenomenon for $[M(SeSiMe_3)_x]^-$ metallates that contain a central atom and do not show a dipole momentum.

2.3 NMR Spectra of PPN[Sn(SSiMe$_3$)$_3$] (2a-PPN)

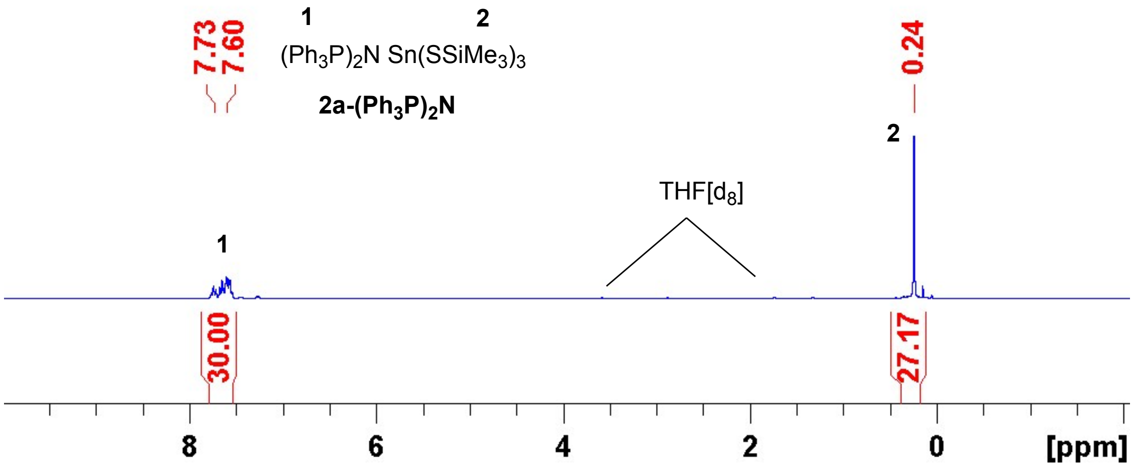

^{1}H-NMR (300.3 MHz, THF[d_8]) of **2a-PPN**.

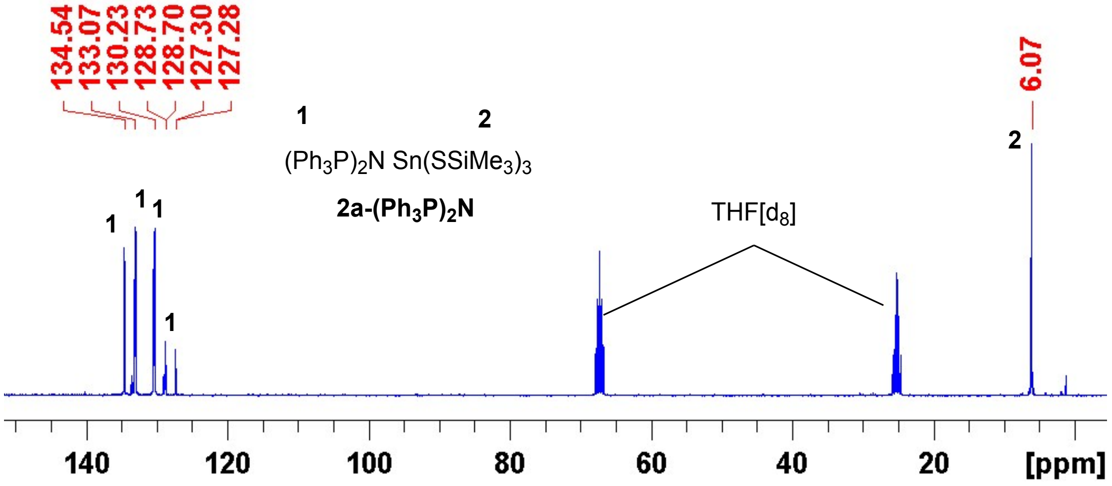

^{13}C{^{1}H} **NMR** (75.5 MHz, THF[d$_8$]) of **2a-PPN**.

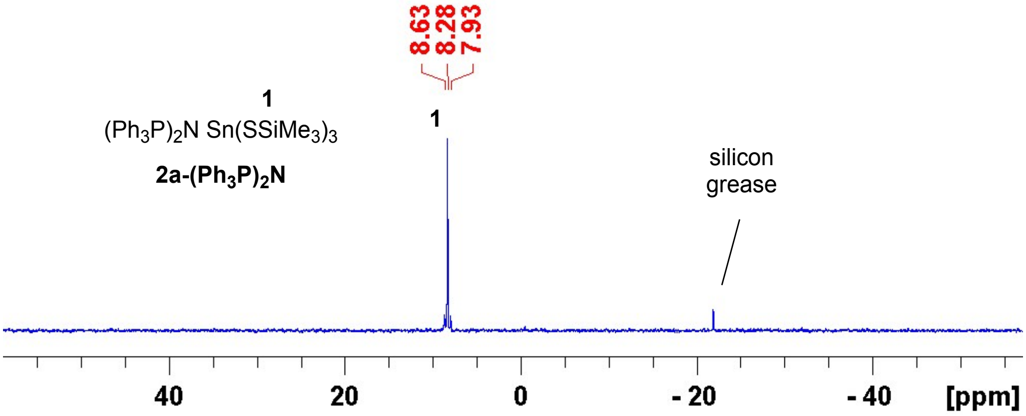

^{29}**Si-NMR** (59.7 MHz, THF[d$_8$]) of **2a-PPN**.

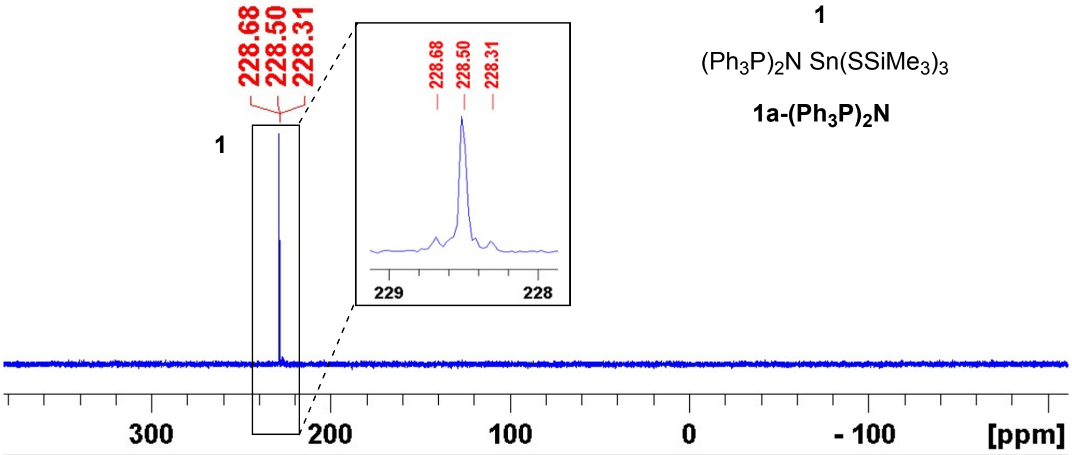

^{119}**Sn NMR** (112.0 MHz, THF[d$_8$]) of **2a-PPN**.

2.4 NMR Spectra of PPN[Sn(SeSiMe$_3$)$_3$] (2b)

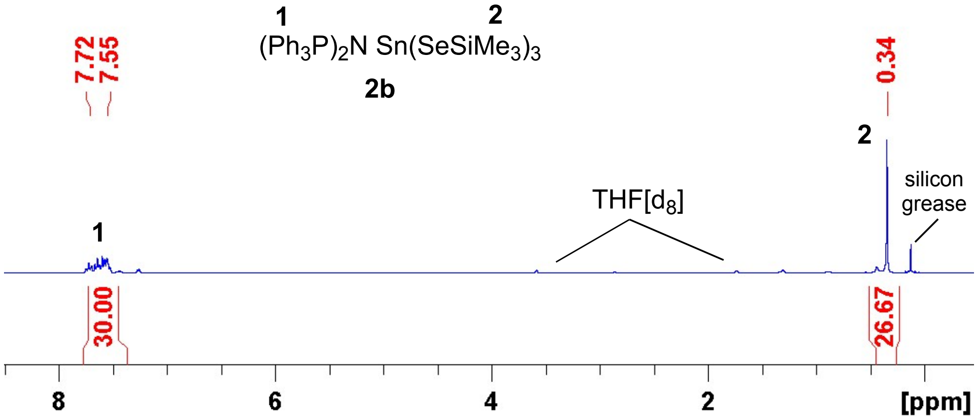

^{1}**H NMR** (300.3 MHz, THF[d$_8$]) of **2b**.

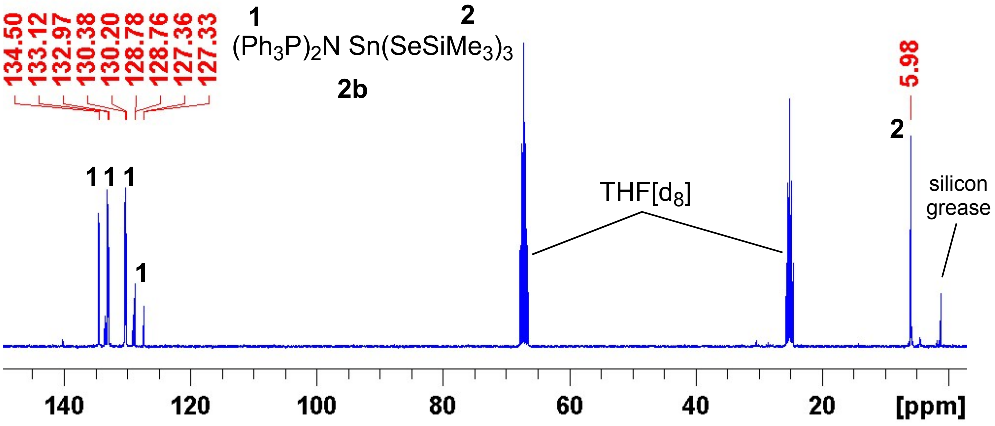

^{13}**C{^{1}H} NMR** (75.5 MHz, THF[d$_8$]) of **2b**.

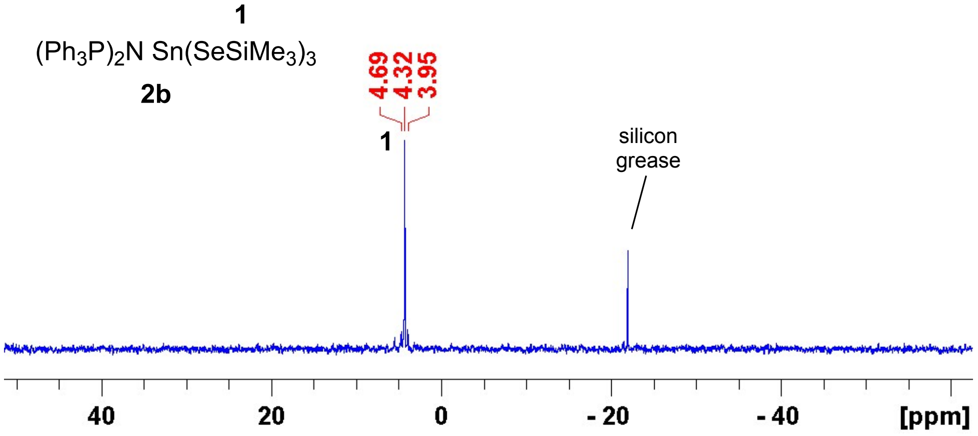

^{29}**Si NMR** (59.7 MHz, THF[d$_8$]) of **2b**.

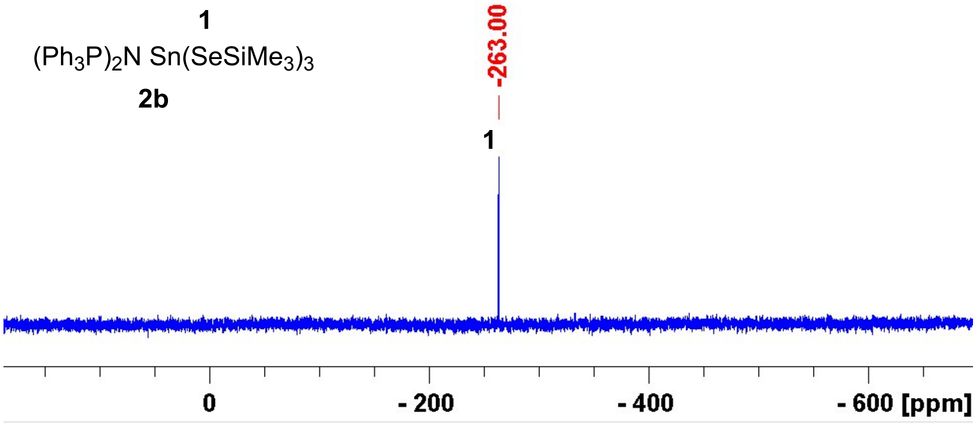

^{77}**Se NMR** (57.3 MHz, THF[d_8]) of **2b**.

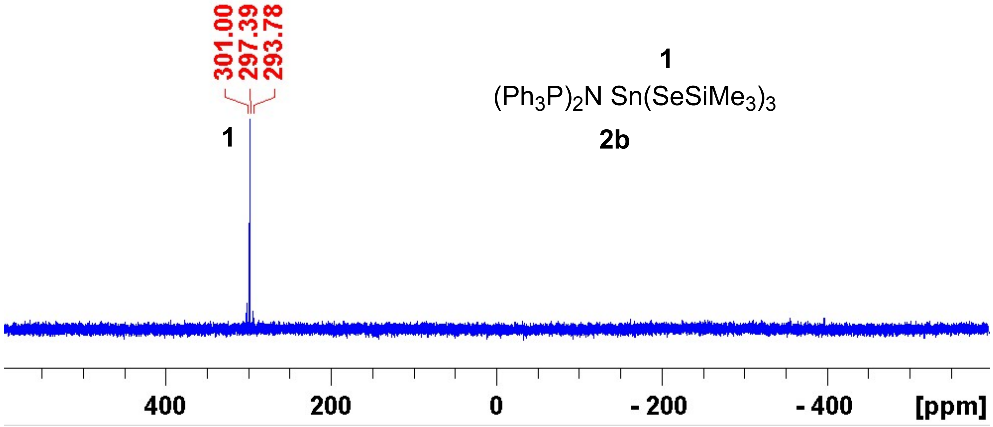

^{119}**Sn NMR** (112.0 MHz, THF[d_8]) of **2b**.

2.5 NMR Spectra of Sn(SSiMe$_3$)$_4$

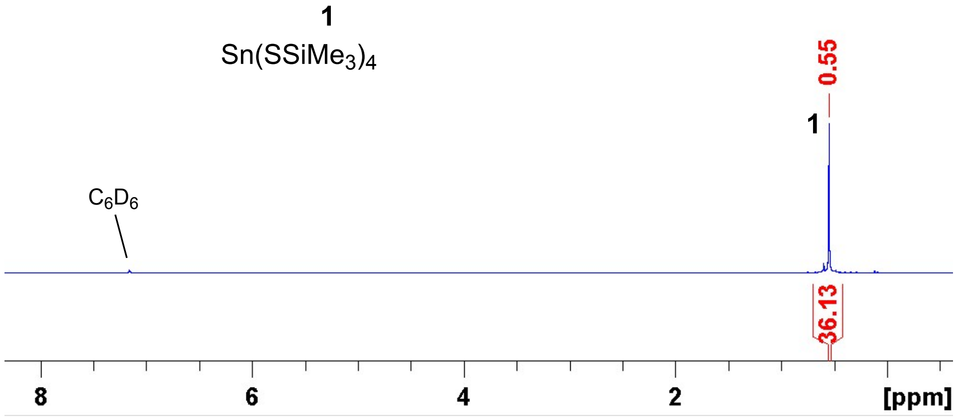

^{1}**H NMR** (300.3 MHz, C_6D_6) of Sn(SSiMe$_3$)$_4$.

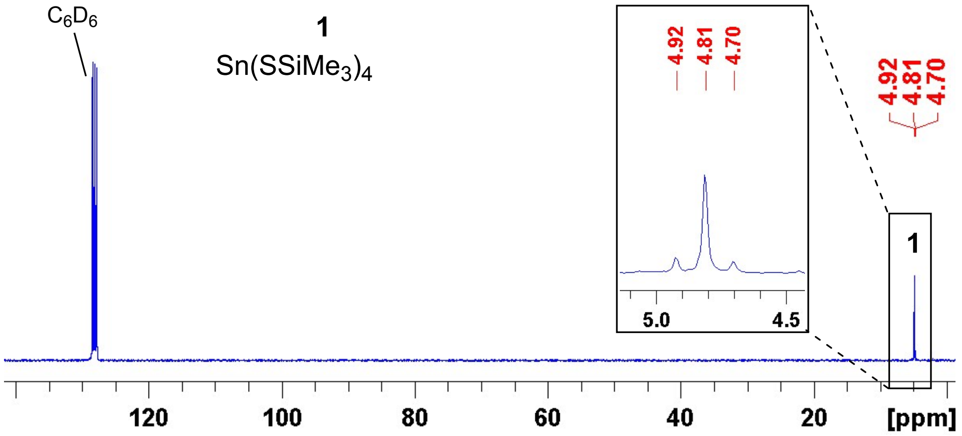

^{13}C{^{1}H} NMR (75.5 MHz, C_6D_6) of $Sn(SSiMe_3)_4$.

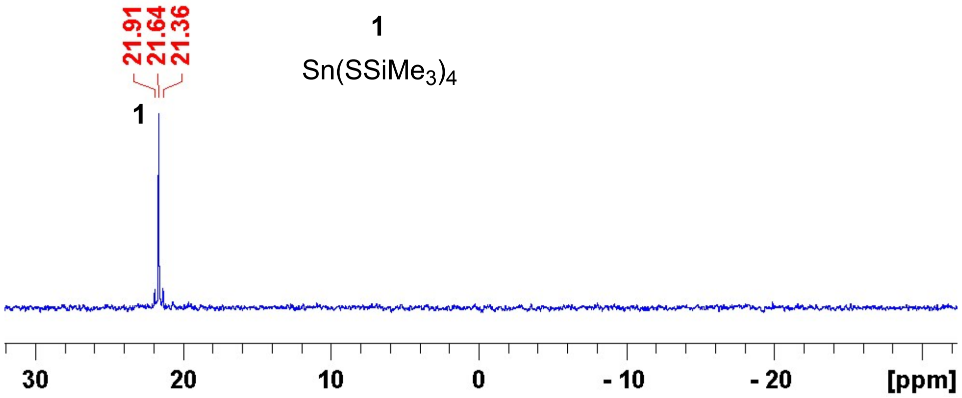

^{29}Si NMR (59.7 MHz, C_6D_6) of $Sn(SSiMe_3)_4$.

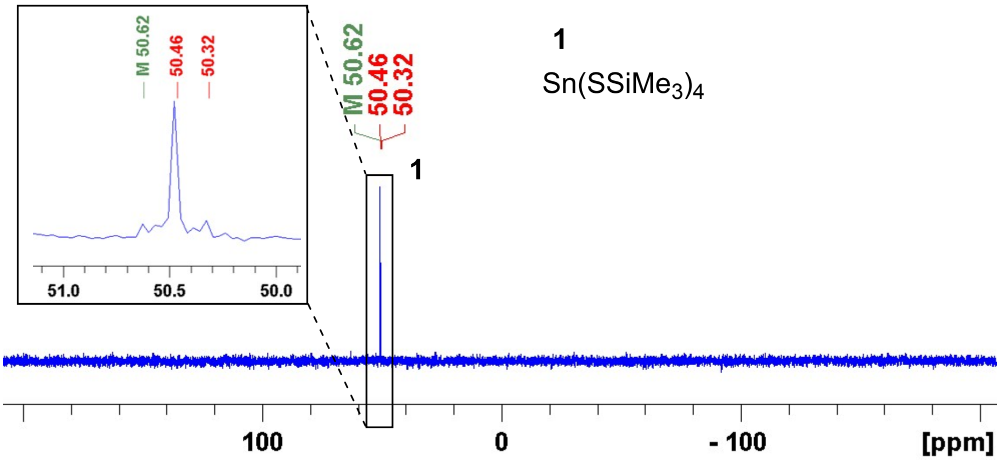

^{119}Sn NMR (112.0 MHz, C_6D_6) of $Sn(SSiMe_3)_4$.

2.6 NMR Spectra of for Sn(SeSiMe$_3$)$_4$

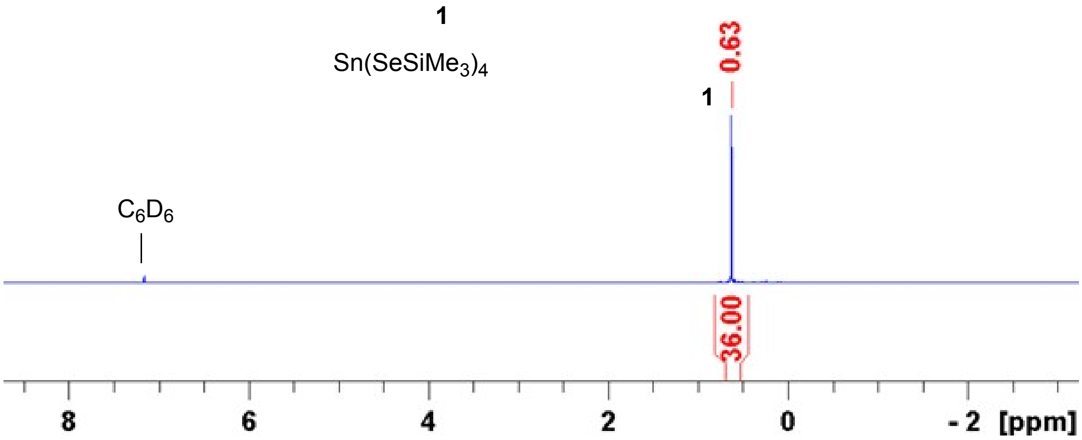

^{1}H NMR (500.2 MHz, C_6D_6) of Sn(SeSiMe$_3$)$_4$.

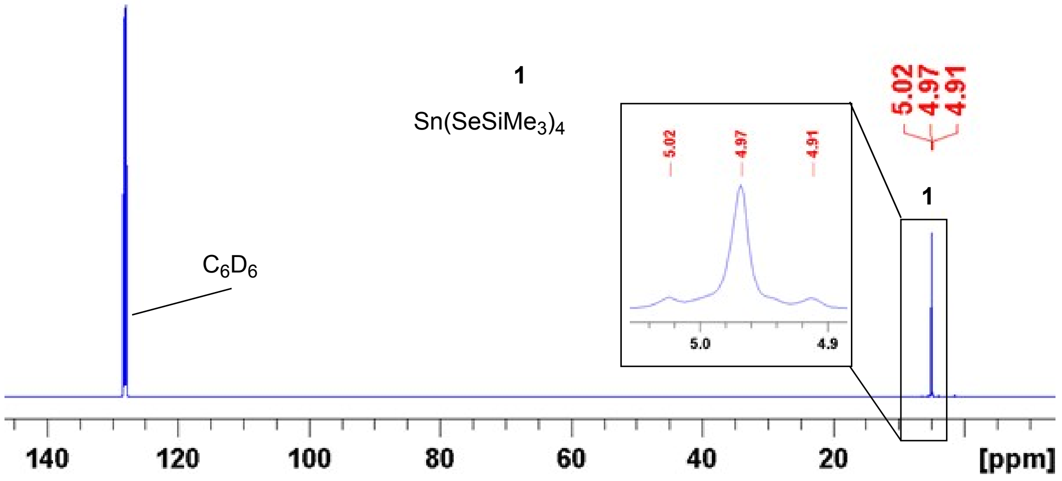

^{13}C{^{1}H} NMR (125.8 MHz, C_6D_6) of Sn(SeSiMe$_3$)$_4$.

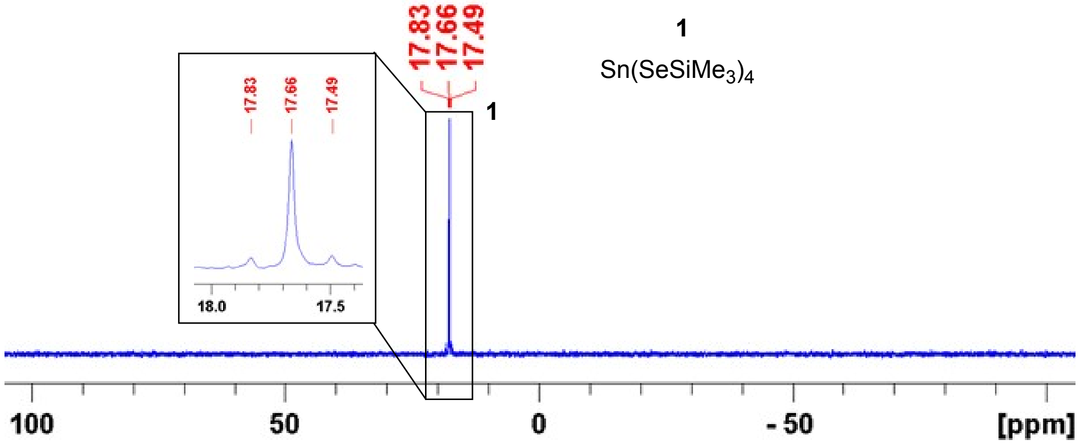

^{29}Si NMR (99.3 MHz, C_6D_6) of Sn(SeSiMe$_3$)$_4$.

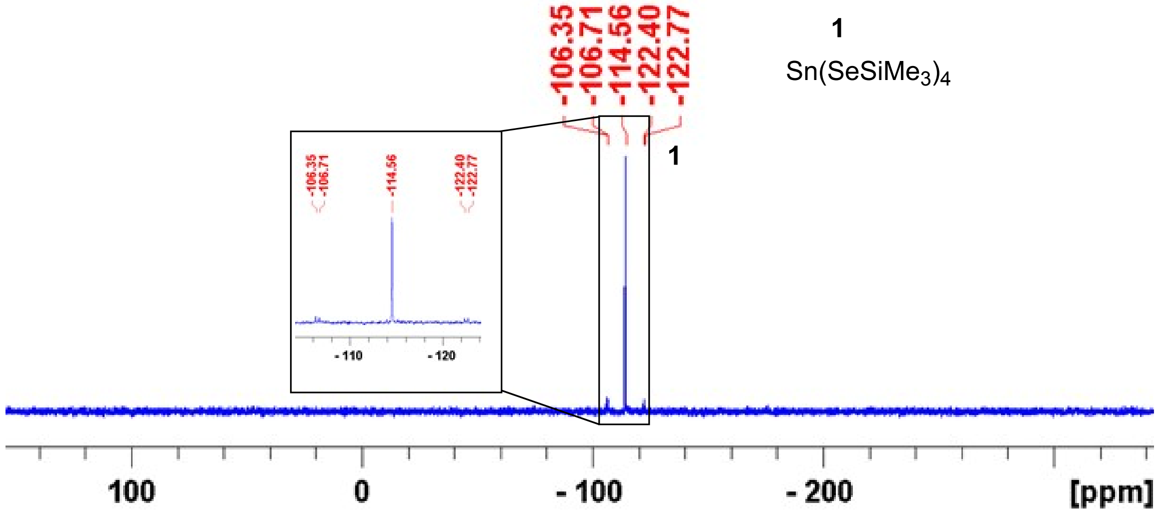

^{77}Se NMR (95.40 MHz, C_6D_6) of $Sn(SeSiMe_3)_4$.

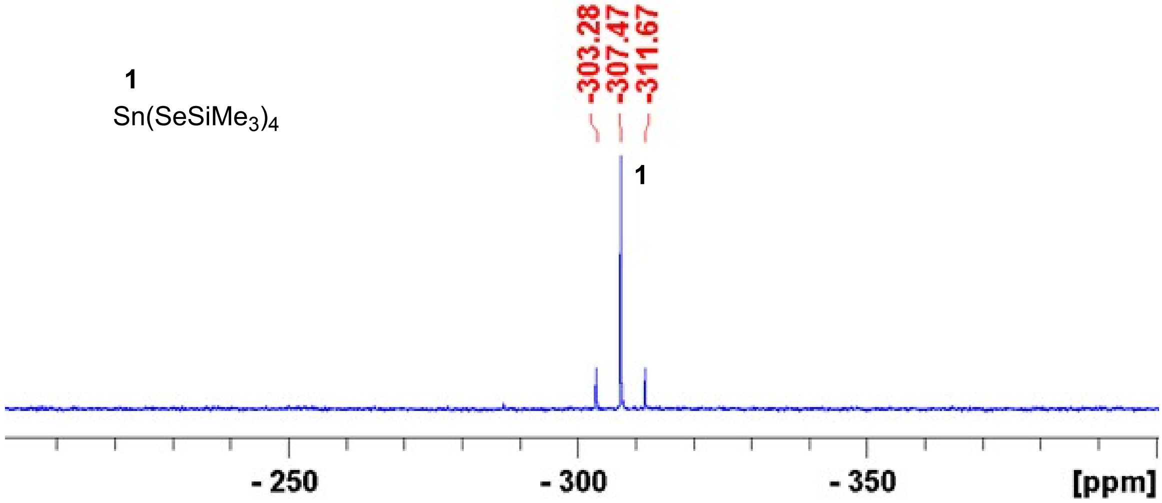

^{119}Sn NMR (186.5 MHz, C_6D_6) of $Sn(SeSiMe_3)_4$.

3. Single crystal XRD data

*3.1 XRD of $Ph_4P[Zn(SSiMe_3)_3]$ (**1a**)*

Table S1: Crystallographic data for $Ph_4P[Zn(SSiMe_3)_3]$ (**1a**).

Identification code	**JG176_0m_a**	
CCDC code	**1940534**	
Empirical formula	C70 H104 O P2 S6 Si6 Zn2	
Formula weight	1515.11	
Temperature	100(2) K	
Wavelength	0.71073 Å	
Crystal system	Monoclinic	
Space group	P 21/n	
Unit cell dimensions	a = 11.687(2) Å	α= 90°.
	b = 18.890(4) Å	β= 98.27(3)°.
	c = 18.770(4) Å	γ = 90°.
Volume	4100.7(15) $Å^3$	
Z	2	
Density (calculated)	1.227 Mg/m^3	
Absorption coefficient	0.902 mm-1	
F(000)	1604	
Crystal size	0.403 x 0.212 x 0.150 mm^3	
Theta range for data collection	2.204 to 27.203°.	
Index ranges	-14<=h<=15, -24<=k<=24, -24<=l<=24	
Reflections collected	50367	
Independent reflections	9097 [R(int) = 0.0320]	
Completeness to theta = 25.000°	99.9 %	
Absorption correction	Semi-empirical from equivalents	
Max. and min. transmission	0.7455 and 0.6684	
Refinement method	Full-matrix least-squares on F2	
Data / restraints / parameters	9097 / 75 / 426	
Goodness-of-fit on F2	1.000	
Final R indices [I>2sigma(I)]	R1 = 0.0284, wR2 = 0.0659	
R indices (all data)	R1 = 0.0385, wR2 = 0.0701	
Largest diff. peak and hole	0.517 and -0.321 e.$Å^{-3}$	

3.2 XRD of $\mathrm{Ph_4P[Zn(SeSiMe_3)_3]}$ (1b)

Table S2: Crystallographic data for $\mathrm{Ph_4P[Zn(SeSiMe_3)_3]}$ (**1b**).

Identification code	**jg280_0m_a**	
CCDC code	**1940535**	
Empirical formula	C66 H94 P2 Se6 Si6 Zn2	
Formula weight	1722.39	
Temperature	100(2) K	
Wavelength	0.71073 Å	
Crystal system	Triclinic	
Space group	P -1	
Unit cell dimensions	a = 12.360(6) Å	α= 104.645(14)°.
	b = 12.641(6) Å	β= 108.529(13)°.
	c = 14.290(7) Å	γ = 105.841(14)°.
Volume	1890.2(17) Å^3	
Z	1	
Density (calculated)	1.513 Mg/m^3	
Absorption coefficient	3.697 mm^{-1}	
F(000)	868	
Crystal size	0.242 x 0.230 x 0.205 mm^3	
Theta range for data collection	2.540 to 25.748°.	
Index ranges	-15<=h<=15, -15<=k<=15, -17<=l<=17	
Reflections collected	53377	
Independent reflections	7214 [R(int) = 0.0633]	
Completeness to theta = 25.000°	99.9 %	
Absorption correction	Semi-empirical from equivalents	
Max. and min. transmission	0.7453 and 0.6145	
Refinement method	Full-matrix least-squares on F2	
Data / restraints / parameters	7214 / 18 / 407	
Goodness-of-fit on F2	1.016	
Final R indices [I>2sigma(I)]	R1 = 0.0285, wR2 = 0.0547	
R indices (all data)	R1 = 0.0426, wR2 = 0.0585	
Largest diff. peak and hole	0.643 and -0.498 e.Å^{-3}	

3.3 XRD of $Ph_4P[Sn(SSiMe_3)_3]$ (2a-Ph$_4$P)

Table S3: Crystallographic data for $Ph_4P[Sn(SSiMe_3)_3]$ (**2a-Ph$_4$P**).

Identification code	**JG174**	
CCDC code	**1940536**	
Empirical formula	C33 H47 P S3 Si3 Sn	
Formula weight	773.81	
Temperature	100(2) K	
Wavelength	0.71073 Å	
Crystal system	Triclinic	
Space group	P -1	
Unit cell dimensions	a = 12.1418(7) Å	α= 110.185(2)°.
	b = 16.0663(9) Å	β= 99.200(2)°.
	c = 22.2417(13) Å	γ = 94.620(2)°.
Volume	3976.6(4) Å^3	
Z	4	
Density (calculated)	1.293 Mg/m^3	
Absorption coefficient	0.951 mm^{-1}	
F(000)	1600	
Crystal size	0.294 x 0.163 x 0.140 mm^3	
Theta range for data collection	2.195 to 25.027°.	
Index ranges	-14<=h<=14, -19<=k<=17, 0<=l<=26	
Reflections collected	14140	
Independent reflections	14140, the crystal was solved as non-merohedral twin.	
Completeness to theta = 25.000°	99.9 %	
Absorption correction	Semi-empirical from equivalents	
Max. and min. transmission	0.745264 and 0.683693	
Refinement method	Full-matrix least-squares on F2	
Data / restraints / parameters	14140 / 24 / 790	
Goodness-of-fit on F2	1.075	
Final R indices [I>2sigma(I)]	R1 = 0.0304, wR2 = 0.0637	
R indices (all data)	R1 = 0.0386, wR2 = 0.0669	
Largest diff. peak and hole	0.416 and -0.797 e.Å^{-3}	

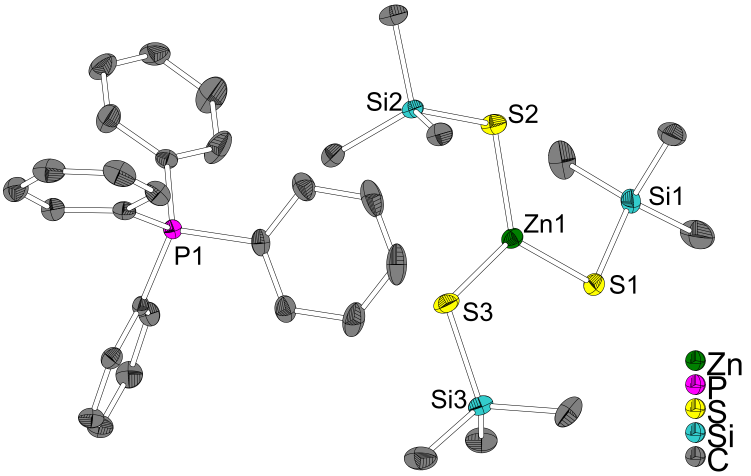

Figure S4: Molecular structure of $Ph_4P[Zn(SSiMe_3)_3]$ (**1a**). Half an equivalent of Et_2O, and hydrogen atoms are omitted for clarity. Relevant bond distances and angles: Zn1-S1: 2.2543(7) Å, Zn1-S2: 2.2536(8) Å, Zn1-S3: 2.2534(7) Å, S1-Si1: 2.1240(8) Å, S2-Si2: 2.1176(7) Å, S3-Si3: 2.1055(9) Å, S1-Zn1-S2: 120.64(2)°, S2-Zn1-S3: 117.65(2)°, S3-Zn1-S1: 121.72(2)°, Zn1-S1-Si1: 104.42(3)°, Zn1-S2-Si2: 105.12(2)°, Zn1-S3-Si3: 108.95(2)°.

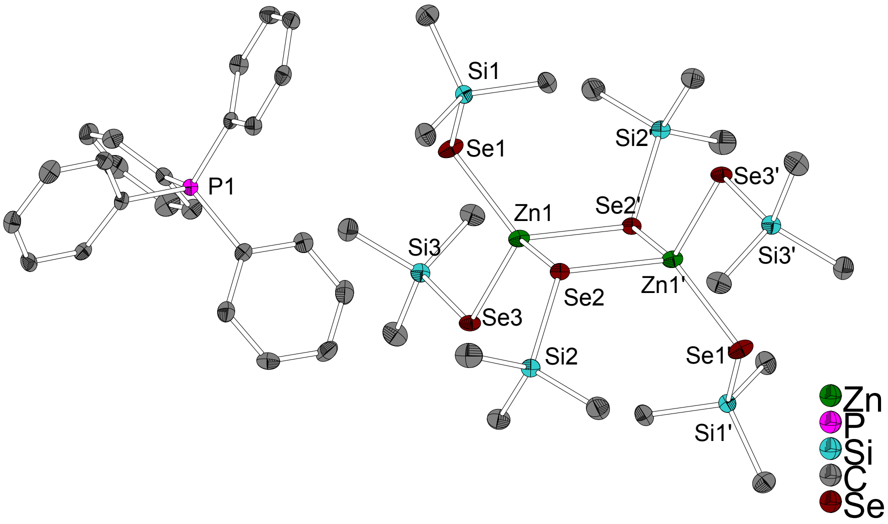

Figure S5: Molecular structure of $Ph_4P[Zn(SeSiMe_3)_3]$ (**1b**). Hydrogen atoms and one Ph_4P-cation are omitted for clarity. Relevant bond distances and angles: Zn1-Se1: 2.414(1) Å, Zn1-Se2: *2.528(1)* Å, Zn1-Se2’: 2.571(1) Å, Zn1-Se3: 2.447(1) Å, Se1-Si1: 2.243(2) Å, Se3-Si3: 2.243(1) Å, Se2-Si2: 2.273(1) Å, Se1-Zn1-Se2: 115.68(3)°, Se1-Zn1-Se2‘: 119.28(3)°, Se1-Zn1-Se3: 108.72(3)°, Se2-Zn1-Se2‘: 89.66(3)°, Zn1-Se2-Zn1‘: 90.34(3)°, Zn1-Se1-Si1: 109.14(4)°, Zn1-Se2-Si2: 117.03(4)°, Zn1-Se3-Si3: 103.96(4)°.

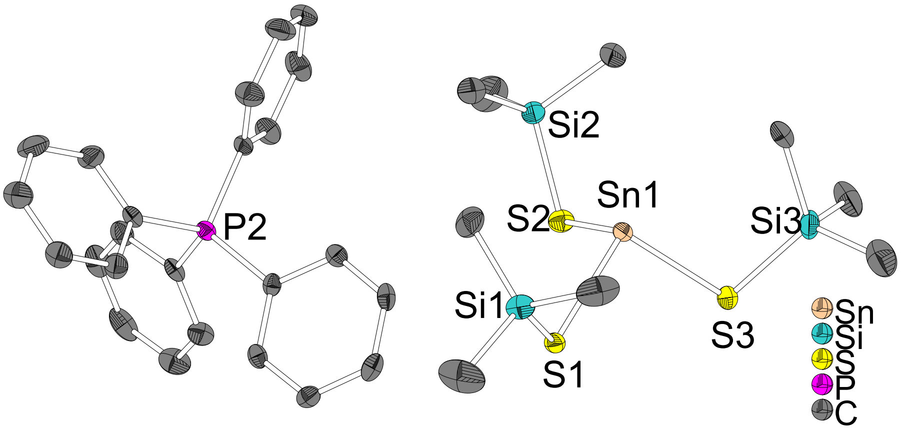

Figure S6: Molecular structure of $Ph_4P[Sn(SSiMe_3)_3]$ (**2a**). Hydrogen atoms and disordered atoms are omitted for clarity. Relevant bond distances and angles: Sn1-S1: 2.5521(9) Å, Sn1-S2: 2.5372(9) Å, Sn1-S3: 2.5366(9) Å, S1-Sn1-S2: 94.24(3)°, S1-Sn1-S3: 94.24(3)°, S2-Sn1-S3: 93.01(3)°, S1-Si1: 2.116(1) Å, S2-Si2: 2.113(1) Å, S3-Si3: 2.114(2) Å, Sn1-S1-Si1: 97.55(4)°, Sn1-S2-Si2: 100.67(5)°, Sn1-S3-Si3: 100.32(5)°.

4. Thermal decomposition of the title anions in form of their Ph_4P and PPN salts

The TGA measurements of the zincates $Ph_4P[Zn(SSiMe_3)_3]$ **1a** and $Ph_4P[Zn(SeSiMe_3)_3]$ **1b** are shown in **Figure 4** in the main text. The residues of the TGA measurements could be identified as ZnS (for **1a**) and ZnSe (for **1b**) via PXRD (**Figure S7**).

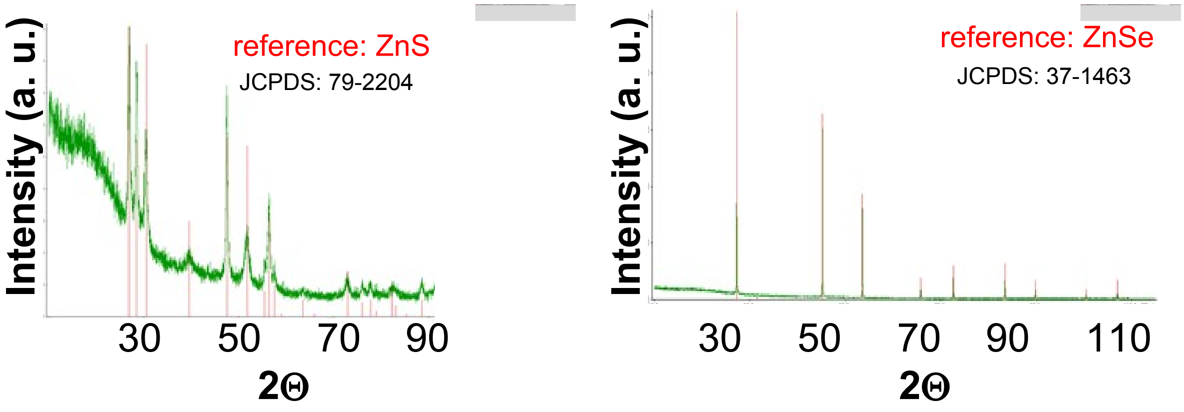

Figure S7: PXRDs of the residues obtained from the TGA measurements of $Ph_4P[Zn(SSiMe_3)_3]$ (**1a**, on the left) and $Ph_4P[Zn(SeSiMe_3)_3]$ (**1b**, on the right). The corresponding binary chalcogenides ZnS (on the left) and ZnSe (on the right) are identified.

The TGA measurements of the stannanides $PPN[Sn(SSiMe_3)_3]$ (**2a-PPN**) and $PPN[Zn(SeSiMe_3)_3]$ (**2b**) are shown in **Figure 5** in the main text. The residues of the TGA measurements could be identified as SnS (for **2a-PPN**) and SnSe (**2b**) via PXRD (**Figure S8**).

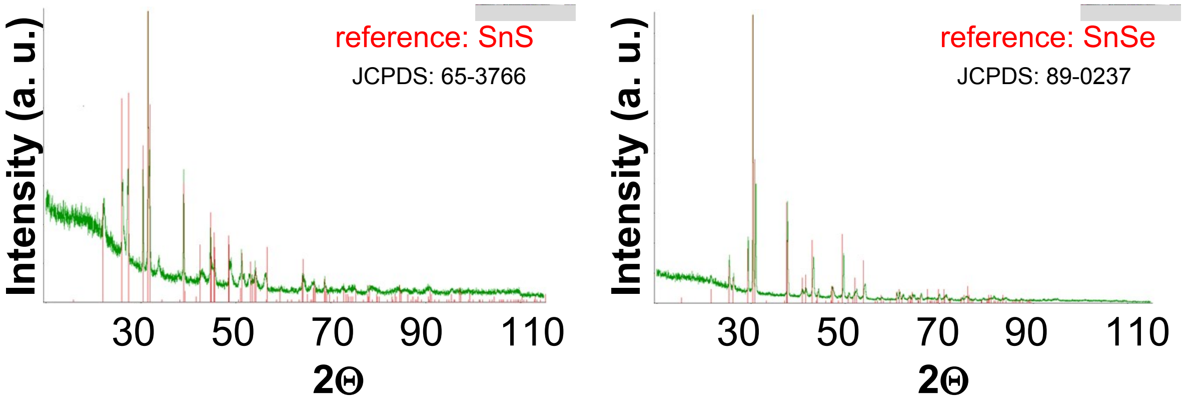

Figure S8: PXRDs of the residues obtained from the TGA measurements of $PPN[Sn(SSiMe_3)_3]$ (**2a-PPN**, on the left) and $PPN[Sn(SeSiMe_3)_3]$ (**2b**, on the right). The corresponding binary chalcogenides SnS (on the left) and SnSe (on the right) are identified.

In order to understand the rather broad temperature range of a complete decomposition of the ionic title complexes into binary chalcogenides, the PPN and $Ph_4P[ESiMe_3]$ salts were prepared for E = S and Se and investigated by TGA. A comparison with corresponding metalates reveals that the broadness of the temperature range of thermal decay of the metalates predominantly originates from the multistep decomposition of the organic cation salts, e.g. $Ph_4P[ESiMe_3]$, formed in a dissociation pre-equilibrium (**Figure S9**).

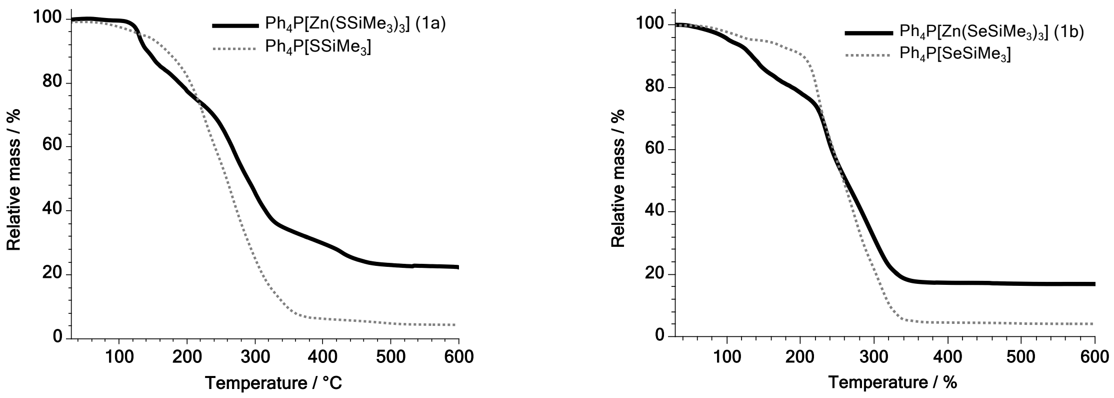

Figure S9: Comparison of the thermal decomposition of the zinkates $Ph_4P[Zn(ESiMe_3)_3]$ with the corresponding organic salts $Ph_4P[ESiMe_3]$ (E = S, left; Se, right).

The decomposition of $Cat[M(ESiMe_3)_{n+1}]$ compounds into $Cat[ESiMe_3]$ and plausible neutral $M(ESiMe_3)_n$ species has been investigated for $Ph_4P[In(ESiMe_3)_4]$ (E = S, Se) by NMR spectroscopy and CHN analysis and was published elsewhere.[2] The $Ph_4P[ESiMe_3]$ compounds decay almost completely into volatiles at 500°C (the Se homologue decomposes slightly faster) with very little residual mass around 5%. The corresponding neutral compounds $M(ESiMe_3)_n$ decompose by condensation induced by elimination of $E(SiMe_3)_2$. While stable intermediates $M(E)_{0.5x}(ESiMe_3)_{n-x}$ might emerge, the complete desilation yield the binary metal chalcogenides $ME_{0.5n}$. This is in accordance with our observations and provides a possible explanation for the outcome of the TGA measurements.

5. Procedure for the preparation of CZTS

Preparation of the Zn/S-precursor mix (**Scheme S1**, **A**): A mixture of $ZnCl_2$ (21 mg, 0.15 mmol, 1.0 equiv.) and PPN [Cl] (89 mg, 0.15 mmol, 1.0 equiv.) is stirred in thf

(10 mL) for 18 h at ambient temperature. In a separate reaction tube, to a solution of $S(SiMe_3)_2$ (84 mg, 0.47 mmol, 3.1 equiv.) in thf (5 mL) a solution of 2.9M *n*-BuLi in hexane (0.16 mL, 0.46 mmol, 3.0 equiv.) is added dropwise at 0 °C. The reaction mixture is stirred for 30 min at 0 °C and further 30 min at ambient temperature. All volatiles are removed under fine vacuum. The obtained colourless powder is directly dissolved in thf (10 mL) and slowly added to the above solution of PPN $[ZnCl_3]$ in thf (10 mL) at –78 °C. The reaction mixture is stirred for 18 h within the cooling bath. During this time the reaction mixture is allowed to slowly reach ambient temperature. A clear, colourless solution of PPN$[Zn(SSiMe_3)_3] \cdot 3$ LiCl in thf (20 mL) is obtained.

Preparation of precursor mix Sn/S (Scheme S1, B): A mixture of $SnCl_2$ (29 mg, 0.15 mmol, 1.0 equiv.) and PPN[Cl] (89 mg, 0.15 mmol, 1.0 equiv.) is stirred in thf (10 mL) for 18 h at ambient temperature. To a solution of $S(SiMe_3)_2$ (84 mg, 0.47 mmol, 3.1 equiv.) in thf (5 mL) a solution of 2.9M *n*-BuLi in hexane (0.16 mL, 0.46 mmol, 3.0 equiv.) is added dropwise at 0 °C in a separate reactor. The reaction mixture is stirred for 30 min at 0 °C and a further 30 min at ambient temperature. All volatiles were removed under fine vacuum with the help of diethyl ether and pentane. The obtained colourless powder is dissolved in thf (10 mL) and slowly added to the solution of PPN$[SnCl_3]$ in thf (10 mL) at –78 °C and the reaction mixture is stirred for 18 h within the cooling bath. During this time the reaction mixture is allowed to slowly reach ambient temperature. A clear, colourless solution of PPN $[Sn(SSiMe_3)_3] \cdot 3$ LiCl in thf (20 mL) is obtained. To this solution a solution of elemental sulfur (5 mg, 0.15 mmol, 1.0 equiv.) in thf (5 mL) is added slowly at –78 °C and stirred for 30 min at this temperature until a green solution is obtained. The mixture is warmed up to ambient temperature and stirred for 1 h. A beige precipitate is obtained. All volatiles were removed in fine vacuum to obtain precursor mix **B**.

Preparation of the multinary sulfidometalate precursor mixture: To the freshly prepared Sn/S precursor mix **B** a solution of Zn/S precursor mix **A** in thf (20 mL) is added and stirred for 10 min at ambient temperature. All volatiles are removed in fine vacuum until a colourless slurry is obtained. This slurry is heated up to 160 °C for 15 min at 10^{-2} mbar until no more volatiles emerge and a yellow-greenish melt arises. When this mixture is cooled down to ambient temperature a beige varnish-like solid is obtained, which is suspended in MeCN (10 mL). A solution of $[Cu(tmtu)_3]PF_6$ (187 mg, 0.31 mmol, 2.0 equiv.; scheme 2, **C**) in MeCN (10 mL) is added slowly at –20 °C. A spontaneous precipitation of black particles is observed. The mixture is stirred at –20 °C for 1 h, warmed to room temperature and stirred for a further 18 h at ambient temperature, while the precipitation intensifies. All volatiles are removed under reduced pressure and the black residue is suspended with diglyme (10 mL). The suspension is annealed at 160 °C without stirring for 5 d. The suspension is centrifugated and the supernatant is removed via canula. The black residue is washed with MeCN (10 mL), then washed with thf (10 mL) and the black solid is dried in fine vacuum. This residue is annealed at 300 °C under N_2 for a further 18 h and then investigated by PXRD and Raman spectroscopy, see **Figure S10** (below).

5.1 Suggested optimized procedure for CZTS co-precipitation

It is suggested to use cheaper quaternary ammonium cations "Cat" and not to separate LiCl from *in situ* generated highly reactive species. Sulfur (1/8 S_8 eq.) as oxidant is added to $Cat[Sn(SSiMe_3)_3]\cdot 3LiCl$ *in situ* formed in diglyme to yield a dispersion of Sn(IV) chalcogenide particles. $Cat[Zn(SSiMe_3)_3]\cdot 3LiCl$ is prepared *in situ* in diglyme. Both dispersions are combined on a target and the third solution of $[Cu(tmtu)_3]PF_6$ in diglyme is printed or spray coated on top. The thin film with precipitating nano- and microparticles is thermally annealed at 160°C under the flux of diglyme under inert conditions. Side products such as LiCl and tmu are very soluble in diglyme and are rinsed in washing steps. Annealing of the dried co-precipitate should lead to CZTS. Both, $(Me_3Si)_2E$ and its activated form $Cat[ESiMe_3]$ (E = S, Se) may be added if extra sources of sulfur and selenium are required in such solvent based precipitation and annealing process. According to TGA, excess $Cat[ESiMe_3]$ salts are decomposed with very little residual mass, as discussed above and in the main text. The suggested steps to be further developed into a printed electronics technology are presented in **Scheme S1.**

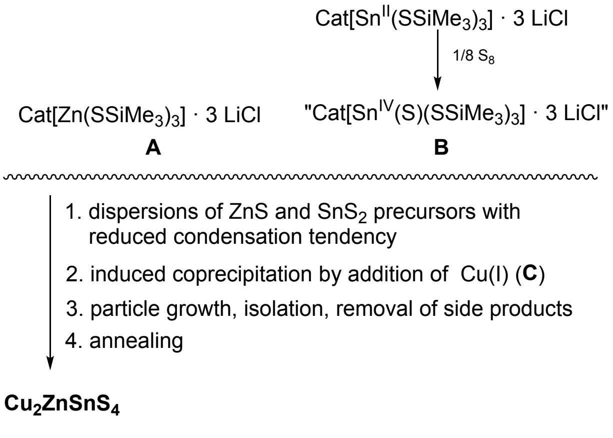

Scheme S1. Procedure to prepare CZTS by using a Cu(I) source **C** and precursor mixtures **A** and **B** prepared from the title anions.

5.2 Discussion of the PXRD data and Raman spectra of CZTS

The identity of CZTS cannot be proven by PXRD exclusively as this compound is known to show essentially the same PXRD pattern as ZnS in the Wurtzite modification.[6]

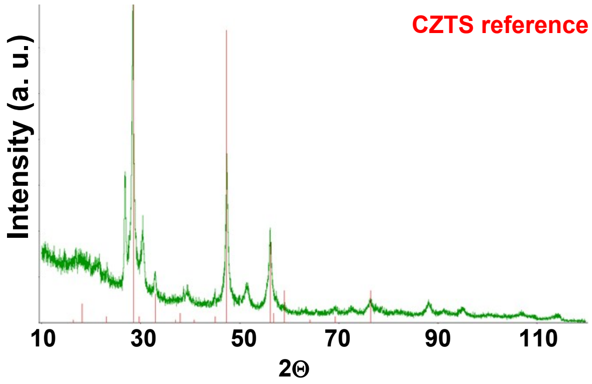

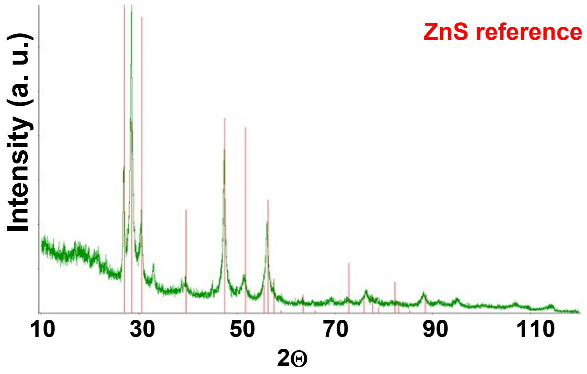

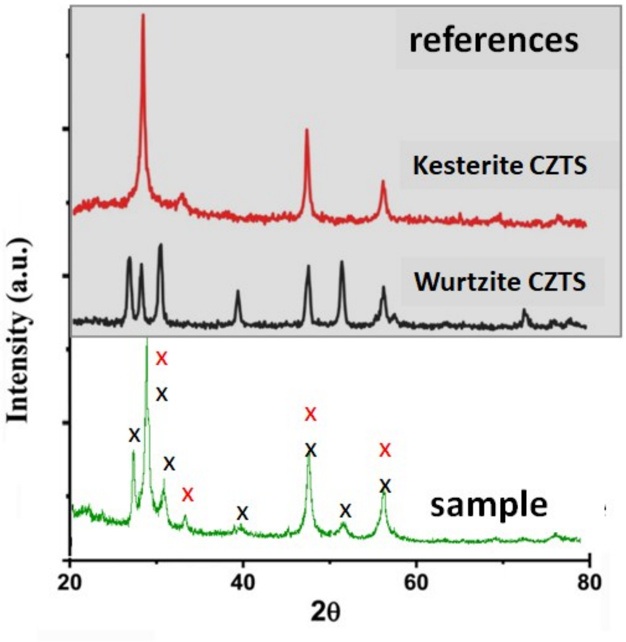

Figure S10: PXRD of the prepared CZTS sample (green diffractogram), top row: with Kesterite Cu_2ZnSnS_4 ref. (JCPDS: 26-0575), middle row: with Wurtzite ZnS ref. (JCPDS: 79-2204) [6b], bottom: two-phase overlay.

The Raman spectrum CZTS shows a strong mode at 336 cm^{-1}, and a small one at 287 cm^{-1}. The absence of a mode at 351 cm^{-1} that is attributed to the first-order Raman mode of w-ZnS, is reported to be an indicator for CZTS to be predominantly present.[6] In the Raman spectrum of the prepared sample (**Figure S11**) no peak at 351 cm^{-1} and only one broad peak at 336 cm^{-1} is observed. This Raman shift has been reported in literature for samples containing CZTS.[9,10] Though these results seem to be promising, they do not provide any information about defects and phase-purity – as mentioned in the main paper.

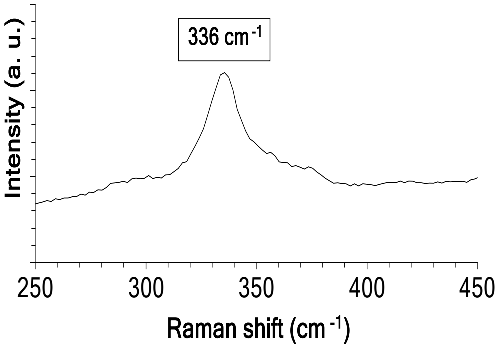

Figure S11: Raman spectrum of the prepared sample.

5.3 Plausible mechanism of condensation of the binary anions to CZTS

It is believed, that dissociation of the metalate complexes Cat[$Zn(SSiMe_3)_3$] and Cat[$Sn(SSiMe_3)_3$], after oxidation by S formally Cat[$Sn(S)(SSiMe_3)_3$], into Cat[$SSiMe_3$] and neutral intermediates [$Zn(SSiMe_3)_2$] and "[$Sn(S)(SSiMe_3)_2$]" triggers the rate of condensation, elimination of $S(SiMe_3)_2$ and formation of a matrix of *in statu nascendi* nanocrystalline particles Cu_2S, ZnS and SnS_2. The proposed mechanism is illustrated in **Scheme S2**. The dissociation of $[M(ESiMe_3)_{n+1}]^-$ anions into $M(ESiMe_3)_n$ and $[ESiMe_3]^-$ has been investigated for $Ph_4P[M(ESiMe_3)_4]$ (M = In; E = S) elsewhere.[2]

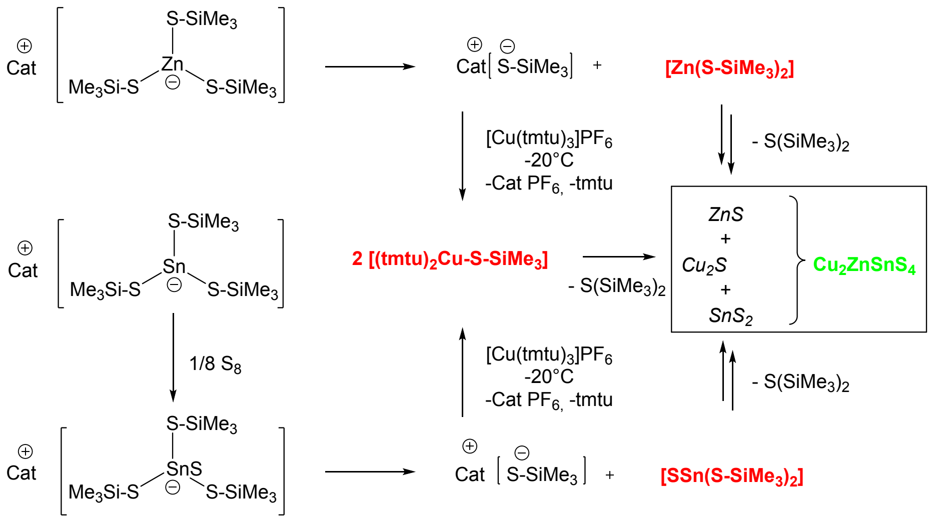

Scheme S2: Proposed mechanism of the coprecipitation of ZnS, Cu_2S and SnS_2 starting from isolated and characterised title metallates.

6. References

(1) T. Shimada, F. S. Ohuchi and B. A. Parkinson, *J. Vac. Sci. Technol. A: Vacuum, Surfaces, and Films*, 1992, **10**, 539–542.

(2) J. Guschlbauer, T. Vollgraff and J. Sundermeyer, *Inorg. Chem.*, 2019, **58**, 15385-15392.

(3) M. Kumar, A. Dubey, N. Adhikari, S. Venkatesan and Q. Qiao, *Energy Environ. Sci.*, 2015, **8**, 3134–3159.

(4) D. Fuhrmann, S. Dietrich and H. Krautscheid, *Chem. Eur. J.*, 2017, **23**, 3338–3346.

(5) D. Fuhrmann, S. Dietrich and H. Krautscheid, *Inorg. Chem.*, 2017, **56**, 13123–13131.

(6) a) X. Yu, A. Ren, F. Wang, C. Wang, J. Zhang, W. Wang, L. Wu, W. Li, G. Zeng and L. Feng, *Int. J. Photoenergy*, 2014, Article ID 861249, 1–6. b) J. Kong, Z. Zhou, M. Li, W. Zhou, S. Yuan, R. Yao, Y. Zhao, S. Wu., *Nanosc. Res. Let.*, 2013, 8, Article No 464 (2013).

(7) M. Himmrich, H. Haeuseler, *Spectrochim. Act.*, 1991, **47A**, 933-942.

(8) S. Kumar, V. Kumar, V. Mikli, T. Varema, M. Altosaar and M. Grossberg, *Energy Procedia*, 2016, **102**, 136–143.

(9) Y. Wang, Y. Huang, A. Y. S. Lee, C. F. Wang and H. J. Gong, *J. Alloys Compd.* 2012, **539**, 237–241.

(10) Z. Seboui, Y. Cuminal and N. Kamoun-Turki, *J. Renew. Sustain. Energy*, 2013, **5**, 23113.